Voltage Stability Improvement in Multi-Terminal HVDC grids: A Case Study of Cigré B4 HVDC Test Grid

Neda Azizi
Department of Electrical Engineering, Razi University
Kermanshah, Iran
neda_azizi71@yahoo.com

Hassan Moradi CheshmehBeigi*
Department of Electrical Engineering, Razi University
Kermanshah, Iran
ha.moradi@razi.ac.ir

Kumarse Rouzbehi
Department of Engineering, University Loyola Andalucía
Seville, Spain
krouzbehi@uloyola.es

Hassan Nouri
Department of Engineering, University of the West of England (UK)
Hassan.Nouri@uwe.ac.uk

***Abstract*— High voltage direct current (HVDC) breaker is among the essential components of HVDC grids. Currently, DC circuit breakers (DCCBs) of HVDC grids require relatively large DC reactors to limit the rate of increase of fault current. However, DC reactors have destructive effects on the multi-terminal HVDC (MT-HVDC) grid dynamic stability, and in such a system, despite the variety of controllers, the system dynamics are highly sensitive to the operating point. This paper proposes a modification to be applied to the droop control of Multi-terminal HVDC (MT-HVDC) grids for stabilizing the DC voltage and power variations in case of transient events by the introduction of a Dead Band Direct Current Power System Stabilizer (DBDC-PSS). Also, this paper presents the classification of MT-HVDC grid dynamic behavior in different scenarios including without DC-PSS, conventional DC-PSS, and DBDC-PSS. All simulations and analytical studies are conducted on Cigré DCS3 test HVDC grid in MATLAB/Simulink.**

***Keywords*— Direct Current Power System Stabilizer (DC-PSS), Dead Band Direct Current Power System Stabilizer (DBDC-PSS), DC voltage stability, Multi-terminal HVDC grids, stability**

I. INTRODUCTION

Power transmission in the form of HVDC high voltage direct current in some cases is preferred to AC transmission [1]. These cases include the use of submarine cables longer than 30 km, due to the high capacitance of AC cables, communication of two alternating current systems with different nominal frequencies, and in power transmission over long distances of more than 600 km [1]. The first commercial use of HVDC transmission between mainland Sweden and the island of Gotland took place in 1954. Since then, the use of a HVDC transmission system has been increasing [1]. With the invention of thyristor converters, HVDC transmission became more attractive. The first HVDC system to use thyristor converters was the Il River project. This project commissioned in 1972, which established a 320-megawatt direct current connection between the power systems of New Brunswick and Quebec, Canada [2]. In recent years, a multi-terminal HVDC transmission network (MT-HVDC) has been used to connect offshore wind farms to the classic AC power system [5]. A review of previous research shows that there are serious concerns about the transient stability of such a network in the event of a fault [6]. Also, HVDC transmission performance is affected by faults on the DC line, converters, or AC system. The effect of the fault is reflected through the converter controllers. So, additional controllers are necessary to provide proper attenuation in such networks [6]. Fault correction for HVDC systems is currently done by AC circuit breakers (ACCB) [7]. However, in the case of HVDC networks, this solution is not possible, because using ACCBs all the energy of the HVDC network must be discharged. Therefore, a DC circuit breaker (DCCB) is required to isolate faulty lines in the HVDC network. However, due to the high cost of this equipment, it is necessary to keep the circuit breaker current as low as possible, so relatively large series reactors along with DC circuit breakers are used to limit the fault current. These large reactors affect voltage control and thus can compromise voltage stability and therefore the stability of the entire AC/DC hybrid network [8].

In an AC network, frequency is used as the synchronization parameter. While in direct current networks, DC voltage can be considered as the synchronization parameter. In fact, in AC/DC hybrid networks, AC/DC converters act as AC side-to-DC voltage interpreters and DC/AC converters act as DC-side voltage-to-AC frequency interpreters. Frequency in an AC network and DC voltage in a HVDC network show changes in grid energy, because changes in AC network frequency or DC voltage in the HVDC network indicate the difference between power output and demand [9-10].

DC voltage stability is interpreted as one of the main control parameters in DC networks. The main purpose of DC voltage control is to maintain the voltage of all terminals within an acceptable range in the event of a transient power imbalance in the MT-HVDC network.

Different strategies for controlling and improving the stability of HVDC networks can be classified into two types. These types include of conventional control methods and advanced intelligent control methods [11]. Similarly, in terms of the type of oscillations, they can be classified into several categories of oscillations, including power/frequency oscillations, asynchronous oscillations, and DC oscillations [12-15]. Mathematical models besides examination of AC/DC

systems are studied in [16]. A VSC-HVDC model is extracted in [17] and DC voltage control and power distribution in a HVDC system based on droop control in [18] are presented.

Dead band controllers are often used to reduce operating and maintenance costs of mechanical devices such as turbine governors in AC systems. The importance of dead bands in AC systems is in regulating the initial frequency and stability. Other uses for dead bands include the use of this equipment in stabilizers [19].

In order to damp low-frequency fluctuations of DC voltage, maintaining frequency voltage balance in AC/DC converters, and power-sharing management in the presence of large reactors, this paper proposes an effective DC-voltage damping controller as Dead Band Direct Current Power System Stabilizer (DBDC-PSS). This controller will have significant impacts on the grid stable operation under grid disturbances and leads to damping of low-frequency fluctuations. Also, to investigate the efficiency of the proposed method alongside the other controllers, several droop controllers are used in the understudy system and the operation of the proposed stabilizer is compared with conventional DC-PSS. Moreover, this paper optimally tunes all the parameters of DBDC-PSS at the same time as a mixed-integer nonlinear optimization programming and solved by Adaptive Particle Swarm Optimization (APSO).

The remaining part of this paper is organized as follows. The network under study is discussed in Section II. Section III is discussed about proposed control strategy. Section IV is deliberated optimization approach and simulation results are shown in section V.

II. NETWORK UNDERSTUDY

The DCS3 Cigre test network is selected for the analysis of the suggested method. Fig. 1 shows the structure of this network. As shown in Fig. 1, the Cigre grid consists of 4 asynchronous AC areas connected by a 5 terminals bipolar MT-HVDC network. This understudy network is included 2 onshore AC systems, 2 offshore AC systems, and 5 VSC-HVDC systems [23-25].

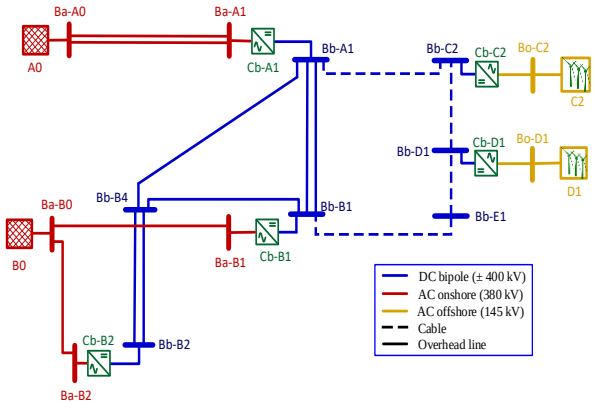

Fig. 1. Cirgre B4 DCS3 test MT-HVDC grid.

It should be mentioned that the standard test network (Cigre DCS3) has only opted as an illustrative test case and the proposed strategy can also be easily applied to any other selected VSC- based HVDC grids. In the current paper, the main goal is to improve the direct voltage stability and decreasing power variations in the events of transients, and this standard grid is selected to confirm the performance and eligibilities of our proposed control strategy. The rated power and voltage for each converter is 1000 MW and ±320 kV. Moreover, it is also assumed that the system has a symmetrical monopole topology.

III. PROPOSED CONTROL STRATEGY

During transient conditions, DC voltages of the MT-HVDC grid will be regulated by the action of the V-P droop control together with the DBDC-PSS to reject the power disturbances coming from other VSC-HVDC stations.

In steady-state conditions, an onshore HVDC station equipped with the HVDC-PSS behaves like a typical converter in the active power control mode. The configuration of this controller is presented in Fig. 2.

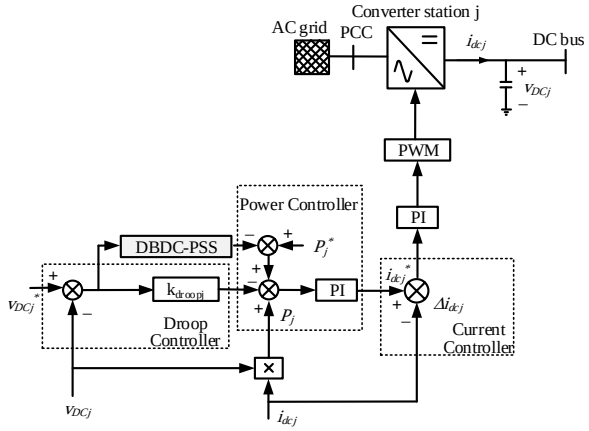

Fig. 2. Structure of V-P droop controller.

The general schematic of the proposed DBDC-PSS controller based on its constituent control blocks is shown in Fig. 3.

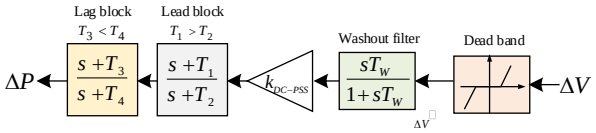

Fig. 3. The general structure of DBDC-PSS.

A DBDC-PSS as a damping controller in a DC system, by injecting an additional signal, improves the stability of the HVDC grid.

The DBDC-PSS controller consists of a wash filter, a lead compensator, a lag compensator again, and a dead band. The washout filter not only allows the V_{DC} oscillations to pass but also prevents the damping controller from reacting to fast dynamics above a certain frequency threshold.

$$\Delta V) = \begin{cases} 0, -dbpss \le \Delta V \le +dbpss \\ \Delta V - dbpss, \Delta V > dbpss \\ \Delta V + dbpss, \Delta V < dbpss \end{cases} \quad (1)$$

The lead-lag compensator is designed to compensate for the phase difference between the DC-PSS output and the converter output power to produce a DC signal component

almost in phase with the V_{DC} signal variations. Also, ΔV^{j} is expressed in (1).

In this paper, it is assumed that the value of *dbpss* is 0.001.

IV. Optimization Approach

This objective function in (2) calculates the area under the curve following the oscillations. Accordingly, the goal is to minimize the E_{dc} parameter as defined in the following:

$$E_{dc} = \sum_{b=1}^{n} \left(\int_{0}^{t} |\Delta V dc| dt \right) \quad (2)$$

However, the problem of optimization of the parameters requires special constraints that all relate to the limits of each of the values and should be taken into account in the optimization problem. The objective function (2) represents the total surface area under DC voltage oscillations, which should be minimized. The definition of the objective function in this way indicates that if there is no perturbation or fault in the understudy system, the value of E_{dc} is zero.

In this paper, our optimization problem is solved by an adaptive particle swarm algorithm (APSO). Its detail and the solution methodology is discussed as follows:

A. PSO algorithm

In the PSO algorithm, first, several particles are randomly selected as the initial population. The situation and speed of any particle are determined by *X* and *V* parameters. The position and velocity of each particle are corrected during the optimization process, according to the current velocity and position and the desired individual position obtained by the particle itself. The information about velocity and the position is informed based on (3) and (4).

$$V_i^{iter+1} = wV_i^{iter} + c_1.r_1.(P_{besti} - X_i^{iter}) + c_2.r_2.(G_{best} - X_i^{iter}) \quad (3)$$

$$X_i^{iter+1} = X_i^{iter} + V_i^{iter+1} \quad (4)$$

In the mentioned equations, *i* indicates the *ith* particle in the swarm. The iteration is shown by iter. Ps represent the best position of the *ith* particle. G_{besti} indicates the best general situation among the swarm. c_1 identified as a cognitive factor and c_2 identified as the social factor. w represents the weight of inertia and r1 and r2 are selected as random numbers between one and zero.

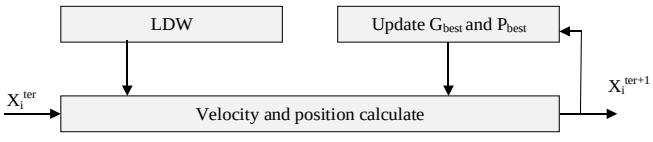

Fig. 4: Block diagram presentation of PSO algorithm.

Fig. 4 shows the block diagram of the PSO algorithm. In the PSO algorithm, the updated linear inertia weight is directly related to the linear decrease in inertia weight (LDW) with increasing repetition time, and LDW is only effective for solving some optimization problems. However, the relationships between inertia weight and repetition time are not always the same for different optimization problems. The search method for practical optimization problems is always nonlinear and very complex, and LDW cannot adapt to complex, nonlinear specifications.

B. APSO algorithm

An adaptive mechanism based on inertia weight is proposed to solve nonlinear optimization problems in the updated inertia weight process. In the process, the weight of adaptive inertia changes dynamically to maintain an acceptable balance between the ability to search the world and particles in the body. Determines the rate of evolution and accumulation of adaptive inertia weight. The evolution rate and degree of aggregation have a great impact on the algorithm.

Optimal local LDW occurs due to the complexity of the problem. Therefore, it is necessary to change the weight of inertia. The rate of evolution and the degree of aggregation show the optimization method between particles, and they show the efficiency of particle motion and the diversity of particles through optimization, respectively. Therefore, a consistent dynamic inertia weight (ADW) is applied to the PSO (APSO). In APSO, the weight of the adaptive inertia varies according to the rate of evolution and the degree of aggregation to achieve an ideal weight for inertia at each repetition. The APSO block diagram is shown in Fig. 5 and forms the feedback control so that it is more reliable and stable than the PSO [20]. Equations (5) and (6) offer this idea.

$$w = f(h, s) \quad (5)$$

$$s = \frac{\min(F(G_{best}^{T}), F_T)}{\max(F(G_{best}^{T}), F_T)} \quad (6)$$

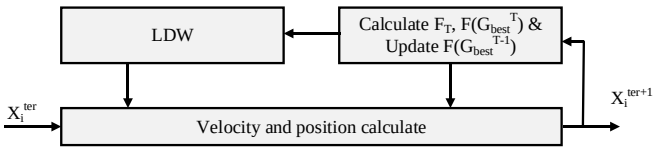

Fig. 5: Block diagram presentation of adaptive PSO.

After slowing down the evolution, the weight of inertia must be reduced so that the particles search in a smaller range and the desired result is found. If the degree of aggregation is scattered, finding the optimal local becomes very complicated. As the degree of aggregation increases, the particles gradually become more easily involved [20].

At this time, the scope of the search space increases to expand the global particle search capability. Finally, the weight of adaptive inertia must decrease with decreasing evolution rate and increase with increasing degree of aggregation. The weight of the increased adaptive inertia is adjusted by (7).

Where the initial value of the weight of inertia is represented by w_{ini}, w_h is the rate of evolution, and w_s is the degree of aggregation. The weight range of adaptive inertia is based on the evolution rate range and the degree of aggregation between w_{ini}-w_h and w_{ini} + w_s. The best w_{ini}, w_h, and w_s standards are 1, 0.5, and 0.05 optionally.

Fig. 6 depicts the flow chart of APSO algorithms with their steps [22].

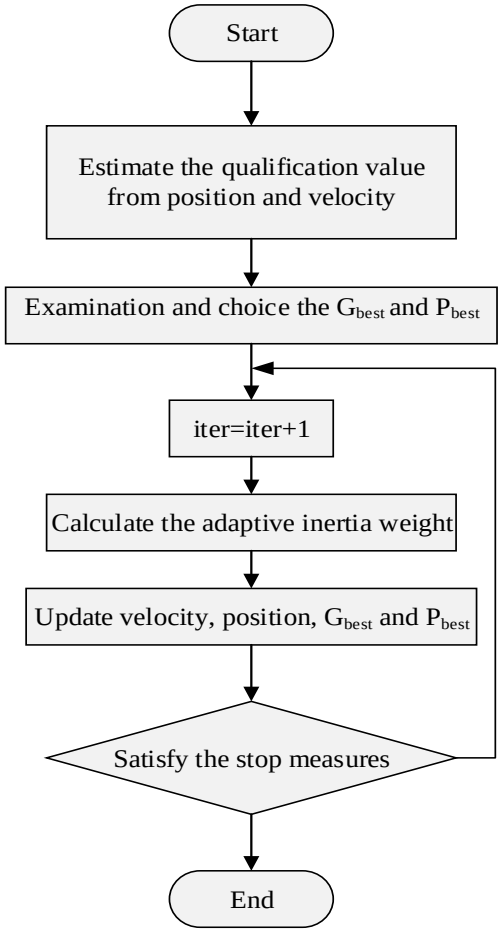

Fig. 6: Flow chart of adaptive PSO algorithm.

$$w = w_{ini} - hw_h + sw_s \quad (7)$$

V. SIMULATION RESULTS

In this part, the proposed DC-PSS for the MT-HVDC test system is assessed.

TABLE I. PARAMETERS OF DC-PSS

Parameter	Optimal value
K_{DC}	125
T_1	0.0211
T_2	0.01
T_3	0.0012
T_4	0.01
T_w	0.1

The suitable values of the DBDC-PSS parameters obtained from APSO are based on the previous analysis listed in Table I.

In these simulations, the DBDC-PSS is applied to the Cb-B2 bus converter. As mentioned before in this study Cigré DCS3 is selected and MATLAB/SIMULINK is used for the simulations.

Responses of the DC voltage and DC power of VDC-Cb-A1, VDC-Cb-B2, VDC-Cb-B1 and PDC-Cb-A1, PDC-Cb-B2, PDC-Cb-B1 under 200 MW reducing of generation in wind farm 2 and during fault happening for 50 ms (3 s–3.05 s) in Cb-A1 bus with droop controller at Cb-B1 and Cb-B2 (kdroop=0.3, kdroop=0.2) without stabilizer, with conventional DC-PSS and with DBDC-PSS is shown as follows.

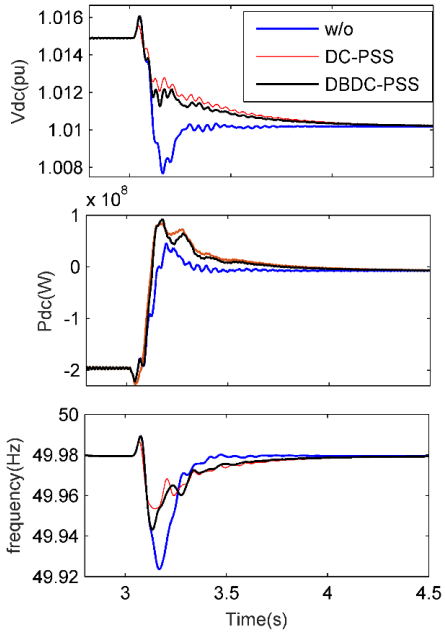

Fig. 7. Direct voltage, DC power, and frequency of AC side of Cb-B1, after changing the power in Cb-A1.

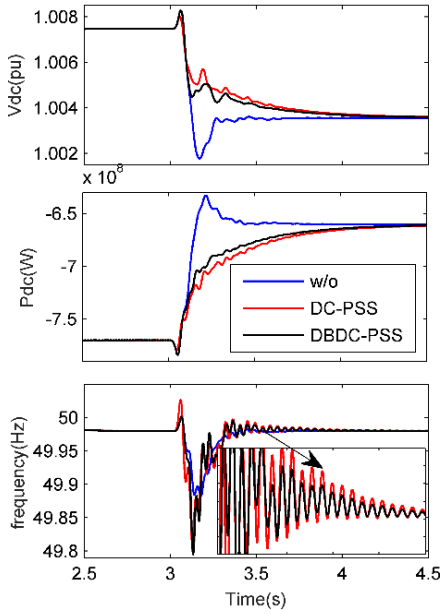

Fig. 8. Direct voltage, DC power, and frequency of AC side of Cb-B2, after changing the power in Cb-A1.

Fig. 7 shows that the presence of DC-PSS along with droop controller reduces the oscillation of voltage at the instant of generation decrease and DC-PSS can reduced the nadir of

signals. Also, Fig. 7 reveals that the network with DBDC-PSS has a better response in transient conditions. Moreover, as shown in this figure, DBDC-PSS has an important effect on the damping of low-frequency oscillations of the frequency of the AC side of the converter.

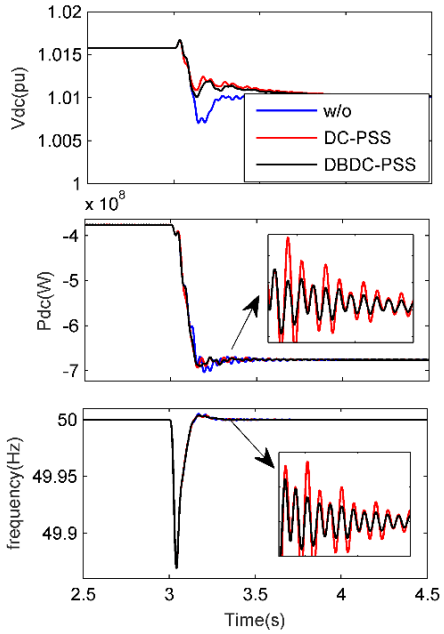

Fig. 9. Direct voltage, DC power, and frequency of AC side of Cb-A1, after changing the power in Cb-A1.

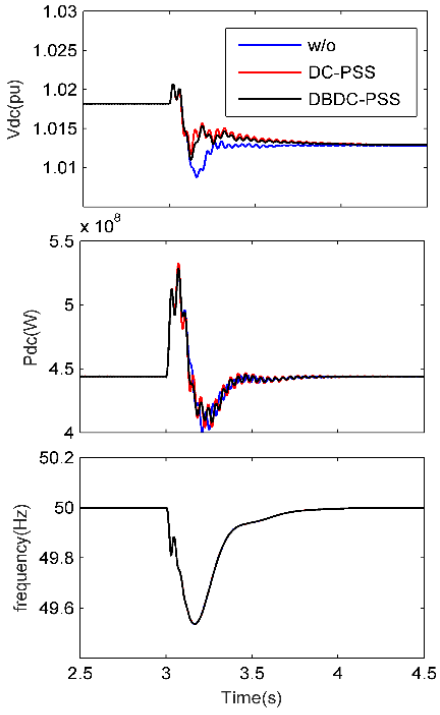

Fig. 10. DC voltage, DC power, and frequency of AC side of Cb-C2, after changing the power in Cb-A1.

Fig. 8 shows the simulation results under the scenario of reduced and increased power production for the Cb-B2 bus.

The results for this bus also confirm that the stability of the direct voltage of Cb-B2 can be improved by using the DBDC-PSS. As shown in Fig. 8, in addition to the voltage, the bus power does not decrease or increase abruptly using the DBDC-PSS and slowly reaches its final value.

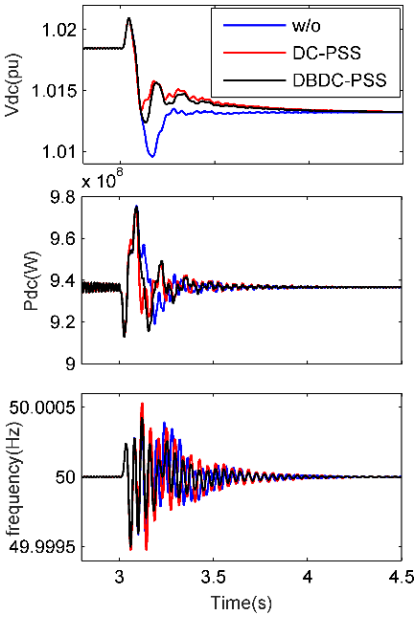

Fig. 11. Direct voltage, DC power, and frequency of AC side of Cb-D1, after changing the power in Cb-A1.

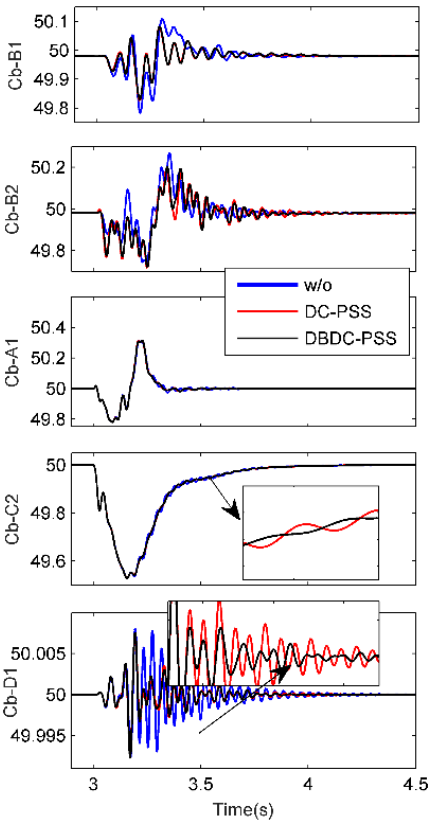

Fig. 12. Frequency of AC side of Cb-A1, Cb-B1, Cb-B2, Cb-C2, and Cb-D1, after a three-phase short circuit in Cb-A1.

The simulation results for the Cb-A1 bus also show in Fig. 9. This figure shows when the power of this bus is randomly and severely fluctuated over a short period, due to the low system inertia, the bus voltage changes drastically.

However, DBDC-PSS has a greater effect on fluctuation damping than conventional DC-PSS. It should be noted that the proposed method has a decent performance in power-sharing and does not impair the performance of the droop controller.

As it is shown in Fig. 9 and Fig. 10, the simulations for these buses repeat the same previous results, except that the controller for these buses is a power controller. So, despite the reduction in output of one bus that reduces the total output power of the system, the power of these busses, after a slight fluctuation, is returned in the reference value.

In addition, Fig. 11 shows that using an inertia loop on the controller can reduce the peak of voltage and DC power fluctuations after change the power output of Cb-A1.

Also, the frequency of the AC side of Cb-A1, Cb-B1, Cb-B2, Cb-C2, and Cb-D1, after a three-phase short circuit in Cb-A1 is shown in Fig. 12. As shown in Fig. 12, since the proposed control loop is applied to the Cb-B2, it appears that the DBDC-PSS has a greater effect on the frequency changes associated.

VI. CONCLUSION

In this paper, in order to increase the dynamic performance of DC voltage control in the MT-HVDC network, the use of the additional stabilizer called DBDC-PSS is proposed. DBDC-PSS is applied on a traditional droop controller. The simulation results confirm that DBDC-PSS can have an acceptable performance following the severe faults or fluctuations in comparison with conventional DC-PSS.

REFERENCES

[1] M. Peker, A. S. Kocaman, and B. Y. Kara, “Benefits of transmission switching and energy storage in power systems with high renewable energy penetration,” Appl. Energy, vol. 228, pp. 1182–1197, Oct. 2018.

[2] P. Rodriguez and K. Rouzbehi “Multi-Terminal DC grids: Challenges and Prospects,” Springer, Journal of Modern Power Systems and Clean Energy, vol. 5, pp 515–523 Jul. 2017.

[3] K. Rouzbehi, G. B. Gharehpetian, J. Candela, A. Luna, L. Harnefors, and P. Rodriguez, “Multi-terminal DC grids: Operating analogies to ac power systems,” Elsevier, Renewable and Sustainable Energy Reviews, vol. 70, pp. 886–895, Apr. 2017.

[4] D. Van Hertem and M. Ghandhari, “Multi-terminal VSC HVDC for the European supergrid: Obstacles,” Renew. Sustain. Energy Rev., vol. 14, no. 9, pp. 3156–3163, Dec. 2010.

[5] T. K. Vrana, J. Beerten, R. Belmans, and O. B. Fosso, “A classification of DC node voltage control methods for HVDC grids,” Electr. Power Syst. Res., vol. 103, pp. 137–144, Oct. 2013.

[6] J. Lilliestam and S. Ellenbeck, “Energy security and renewable electricity trade—Will Desertec make Europe vulnerable to the ‘energy weapon’?,” Energy Policy, vol. 39, no. 6, pp. 3380–3391, Jun. 2011.

[7] J. Jardini, T. K. Vrana, Y. Yang, Dragan, Jovcic, S. Dennetière, J. Jardini and H. Saad, “The Cigré B4 DC grid test system The CIGRE B4 DC Grid Test System B4-58.”, *Electra*, vol. 270, pp. 10-19, 2013.

[8] D. Mueller, M. Rabe, and W. Kuehn, “Stabilizing control for HVDC connected offshore wind farm,” in IEEE PES ISGT Europe 2013, pp. 1–5, 2013.

[9] Y. Taehan Chŏn’gi Hakhoe., J. Zhou, W. Li, J. Zhu, and C. Hong, Journal of electrical engineering & technology., vol. 13, no. 3. Korean Institute of Electrical Engineers, 2018.

[10] B. Berggren, K. Linden, and R. Majumder, “DC Grid Control Through the Pilot Voltage Droop Concept—Methodology for Establishing Droop Constants,” IEEE Trans. Power Syst., vol. 30, no. 5, pp. 2312–2320, Sep. 2015.

[11] E. Prieto-Araujo, A. Egea-Alvarez, S. Fekriasl, O. Gomis-Bellmunt, “DC voltage droop control design for multiterminal HVDC systems considering AC and DC grid dynamics.” IEEE Transactions on Power Delivery., vol. 31, no. 2, pp. 575-85, 2016.

[12] S. Cole, J. Beerten, R. Belmans, “Generalized dynamic VSC MTDC model for power system stability studies.” IEEE Transactions on Power Systems., vol. 25, no. 3, pp. 1655-62, 2010.

[13] K. Rouzbehi, A. Miranian, A. Luna, P. Rodriguez, “DC voltage control and power-sharing in multiterminal DC grids based on optimal DC power flow and voltage-droop strategy.” IEEE Journal of Emerging and selected topics in power Electronics., vol. 2, no. 4, pp. 1171-80, 2014.

[14] W. Wang, M. Barnes, O. Marjanovic and O. Cwikowski, “Impact of DC breaker systems on multiterminal VSC-HVDC stability.” IEEE Transactions on Power Delivery, vol. 31, no. 2, pp.769-779, 2015.

[15] S. D’Arco, J. A. Suul, and J. Beerten. "Configuration and model order selection of frequency-dependent π-models for representing dc-cables in small-signal eigenvalue analysis of HVDC transmission systems." IEEE Journal of Emerging and Selected Topics in Power Electronics, 2020.

[16] J. Beerten, S. D'Arco and J. A. Suul, "Cable model order reduction for HVDC systems interoperability analysis", IET ACDC, pp. 10-12, Feb. 2015.

[17] S. S. H. Yazdi, K. Rouzbehi, J.I. Candela, J. Milimonfared and P. Rodriguez, P. ‘Flexible HVDC transmission systems small-signal modelling: A case study on CIGRE Test MT-HVDC grid’, IECON 2017-43rd Annual Conference of the IEEE Industrial Electronics Society, pp. 256-262, 2017.

[18] Azizi, N., CheshmehBeigi, H.M. and Rouzbehi, K. “Optimal placement of direct current power system stabilizer (DC-PSS) in multi-terminal HVDC grids”. IET Generation, Transmission & Distribution, vol.14, no. 12, pp. 2315-2322, 2020.

[19] Liu, M., Bizzarri, F., Brambilla, A. M., & Milano, F. (2019). On the impact of the dead-band of power system stabilizers and frequency regulation on power system stability. *IEEE Transactions on Power Systems*, vol. 34, no. 5, pp. 3977-3979.

[20] C. Du, Z. Yin, Y. Zhang, J. Liu, X.-D. Sun, and Y. Zhong, “Research on Active Disturbance Rejection Control of Induction Motors Based on Adaptive Particle Swarm Optimization Algorithm with Dynamic Inertia Weight,” IEEE Trans. Power Electron., pp. 1–1, 2018.

[21] T. Jamrus,C.F. Chien, M. Gen and K. Sethanan, "Hybrid particle swarm optimization combined with genetic operators for flexible job-shop scheduling under uncertain processing time for semiconductor manufacturing.", IEEE Transactions on Semiconductor Manufacturing, vol. 31, no. 1, pp. 32-41, 2017.

[22] Z. Ren, A. Zhang, C. Wen and Z. Feng, "A scatter learning particle swarm optimization algorithm for multimodal problems.", IEEE transactions on cybernetics, vol. 44, no. 7, pp. 1127-1140, 2013.

[23] H. R. Wickramasinghe, G. Konstantinou, Z. Li and J. Pou, "Alternate arm converters-based HVDC model compatible with the CIGRE B4 DC grid test system.", IEEE Transactions on Power Delivery, vol. 34, no. 1, pp. 149-159, 2018.

[24] M. Mokhtari and G. B. Gharehpetian, "Integration of energy balance of soil ionization in CIGRE grounding electrode resistance model. IEEE Transactions on Electromagnetic Compatibility, vol. 60, no. 2, pp. 402-413, 2017.

[25] H. Yan, K. Liu, X. Wang, K. Che, Y. Ding, and W. Yang. "Research on CIGRE benchmark model and improved DC control strategy." In Journal of Physics: Conference Series, vol. 1633, no. 1, p. 012080, 2020.